11

Design and Implementation of Reader Baseband Receiver Structure in a Passive RFID Environment

Ji-Hoon Bae[1], Kyung-Tae Kim[2], WonKyu Choi[1] and Chan-Won Park[1]
[1]*Electronics and Telecommunication Research Institute*
[2]*Pohang University of Science and Technology (POSTECH)*
Republic of Korea

1. Introduction

In this chapter, we present a demodulation structure suitable for a reader baseband receiver in a passive Radio Frequency IDentification (RFID) environment. RFID refers to a technology which uses radio communications to contactlessly identify a tagged physical object [1-2]. An RFID system may include a plurality of electronic tags on objects, animals, and other things having unique identification information and a reader for reading or writing information from or to the tags. RFID systems can be variously classified into the inductively coupled and electromagnetic schemes according to the communication method employed between an RFID reader and a tag, into an active type and a passive type according to whether the tag operates using its own power or not, and into long wave, medium wave, shortwave, ultrashort wave, and microwave depending on the frequency of the electric waves used for the communication [1-2]. Essentially, a passive RFID system consists of a reader and a passive tag without a battery. The International standard, ISO 18000-6C, defines the communication protocol and Ultra High Frequency (UHF) band between the reader and the passive tag [3]. Many studies have been conducted in the field of UHF RFID, as described in [4-14]. In the case of passive UHF RFID technology, the reader must provide the tag with continuous radio power, while the tag sends its information to the reader via a backscatter modulation. The tag encodes the backscattered signal as either FM0 (bi-phase space) or Miller modulation of subcarrier at the given data rate [3]. Recently, UHF Passive RFID has a trend of extending its domain to the application of an item-level-tagging (ILT) from that of a conventional pallet/case-level-tagging. In the ILT RFID environment, tags can be attached on the objects composed partially of a metal or liquid and can be placed at a nearby complicated surrounding in which the metallic objects exist. As a result, if undesired large signal reflected from the complicated surrounding is received at the reader receiver during receiving a desired backscattered tag signal, the performance of the identification for the reader can be easily degraded due to the reflected large signal which can leak to the reader receiver (Fig. 1(a)). In addition, if insufficient isolation is guaranteed between the transmitter and receiver, the transmission power (Tx power) created by the reader transmitter can leak to the receiver (Fig. 1(a)) [2]. A reflected power larger than the backscattered tag signal which is generated by the return loss (S11) of the

antenna can also leak to the receiver via the circulator (Fig. 1(a)). Because of these unwanted leakage components in the reader receiver, the DC-offset phenomenon can occur in the baseband of the reader receiver.

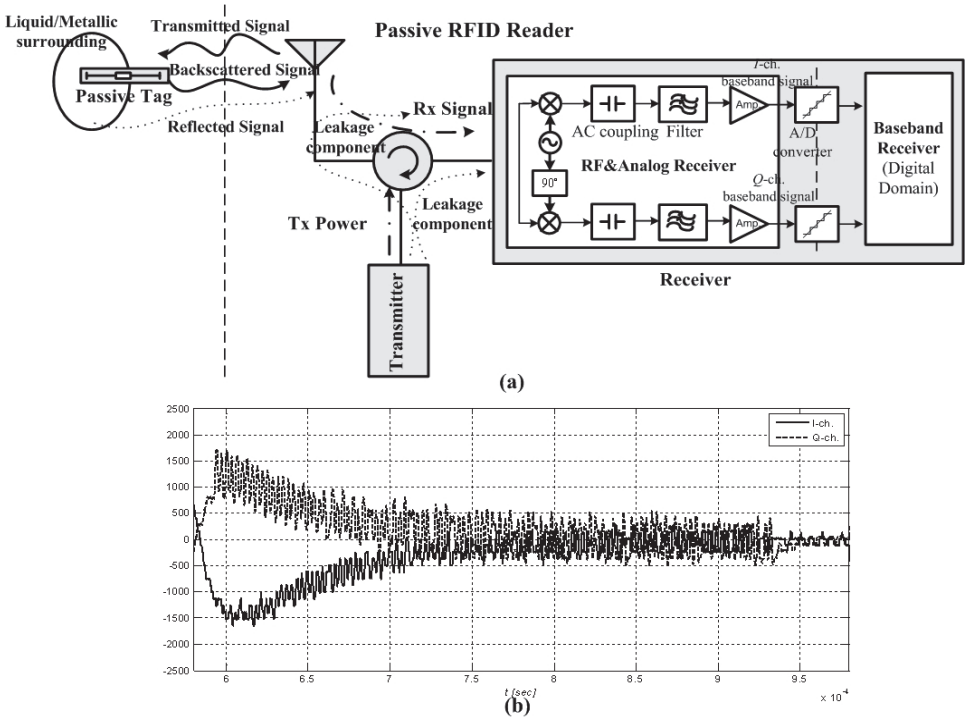

Fig. 1. Description of leakage components (a) and the corresponding DC-offset phenomenon (b) in a passive RFID communication environment

As a result, the received baseband signal can be corrupted by the DC-offset phenomenon (Fig 1(b)). For example, Fig. 1(b) shows the Miller subcarrier signal highly affected by the DC offset phenomenon in our reader receiver measured using an Agilent Logic Analyzer. Due to the unwanted DC-offset phenomenon, the reader baseband receiver may not determine the valid bit data with sufficient reliability. There have been several researches to reduce the originally generated leakage components in advance, as reported in [4-6]. However, it may be difficult to perfectly and adaptively eliminate the leakage components in the ILT RFID field, in which the performance of the reader receiver can be adversely affected by the unwanted large reflected signals. Therefore, although the received baseband signal is contaminated with the DC-offset phenomenon, we attempt to further remove the DC-offset phenomenon from the distorted received signal in the baseband receiver. In the earlier study, we proposed a demodulation structure composed of an edge signal generator, an edge extractor and a signal reconstruction block for the FM0 signal distorted by the DC-offset phenomenon [14]. In this chapter, a similar concept is also applied to the reliable reconstruction of the Miller subcarrier signal not suffering from the DC-offset phenomenon by using the phase inversion information instead of the amplitude information. In order to

accomplish this, we detect the valid information from the corrupted signals by making use of a demodulation structure composed of a peak signal generator, a peak detector, and a signal reconstruction block, in order to successfully decode the received baseband signal distorted by the DC-offset phenomenon. According to the proposed demodulation method, the peak signal is created at the position of phase inversion within the Miller subcarrier signal sequence using the phase inversion information. Therefore, although a certain amount of DC-offset noise can be appeared in the baseband of the reader receiver, the proposed method is allowed to supplementally deal with the DC-offset phenomenon once more in the baseband receiver.
This chapter is organized as follows. In Section 2, we describe in detail the demodulation structure and method used to extract meaningful information from the distorted Miller subcarrier signal suffering from the DC-offset phenomenon. In Section 3, we show the simulation and implementation results. Finally, we draw our conclusions in Section 4.

2. Demodulation algorithm

In this section, we introduce the demodulation structure and algorithm suitable for the reconstruction of the Miller subcarrier signal distorted by DC-offset noise.

2.1 Demodulation of the Miller subcarrier-encoded signal

The Miller modulated sequence contains exactly two, four, or eight subcarrier cycles per bit, depending on the M value (M = 2,4,8) specified in [3]. Namely, if M has a value of 2, the Miller basis signal is multiplied by a square-wave at 2 times the symbol rate ($1/(M \cdot T_b)$), resulting in a Miller subcarrier signal with M = 2, as shown in Fig. 2. For the reliable reconstruction of the Miller subcarrier signal under the DC-offset environmnet, Fig. 3 shows the proposed demodulation architecture, which includes a peak signal generator, a peak extractor, and a signal reconstruction block, similar to the FM0 demodulation structure [14]. As shown in Fig. 3, the received signal, r(t) is composed of an in-phase channel (I-channel) signal, $r_I(t)$, and a quadrature-phase channel (Q-channel) signal, $r_Q(t)$ including DC-offset noise, n_{dc}, and the complex additive noise, $n(t)$, which is a sample function of a white Gaussian process with power spectrum $N_0/2$ watts/hertz. At this point, the DC-offset noise (n_{dc}) can be expressed as follows [14]:

$$n_{dc}(t) = A_{dc} \cdot e^{-B \cdot t} e^{j(w_d \cdot t + \psi)} \tag{1}$$

where A_{dc} is the initial DC-offset value, $e^{-B \cdot t}$ and $e^{jw_d \cdot t}$ represent the damping term and oscillation term of the DC-offset noise, respectively, and $e^{j\psi}$ is the initial phase of the DC-offset noise. By adjusting the parametrs A_{dc}, B, and w_d related to the DC-offset noise to proper values, any kind of DC-offset phenomenon in the area of passive RFID can be established.
In order to generate the peak signal with respect to the received baseband signal r(t) which is sampled at a sampling rate of $1/T_s$, the initial peak signal $r_{p1}(t)$ is designed using the predefined $s_{m0}(t)$ and $s_{m1}(t)$ as follows:

$$r_{p1}(t) = \left[LPF\{r_1(t) - r_0(t)\} \right]_{,t=(k \cdot T_s),k=0,1,2,\ldots} \tag{2}$$

where $r_0(t)$ is the output signal using $s_{m0}(t)$ via the I and Q channels and is defined as follows:

$$r_0(t) = \frac{1}{A}\left(\underbrace{\left| r_I(t) \otimes s_{m0}(t) \right|}_{I-channel} + \underbrace{\left| r_Q(t) \otimes s_{m0}(t) \right|}_{Q-channel} \right), \tag{3}$$

where, A is the normalized gain, and $r_1(t)$ is the output signal using $s_{m1}(t)$ via the I and Q channels and is defined as follows:

$$r_1(t) = \frac{1}{A}\left(\underbrace{\left| r_I(t) \otimes s_{m1}(t) \right|}_{I-channel} + \underbrace{\left| r_Q(t) \otimes s_{m1}(t) \right|}_{Q-channel} \right) \tag{4}$$

$s_{m0}(t)$ has the same form as data-0 of the Miller subcarrier and $s_{m1}(t)$ has the same form as data-1 of the Miller subcarrier [3]. If M is four, then $s_{m0}(t)$ and $s_{m1}(t)$ can be described by Fig. 4. In our method, the low pass filtering of the difference signal between $r_1(t)$ and $r_0(t)$ is required for the generation of the desired peak signal.

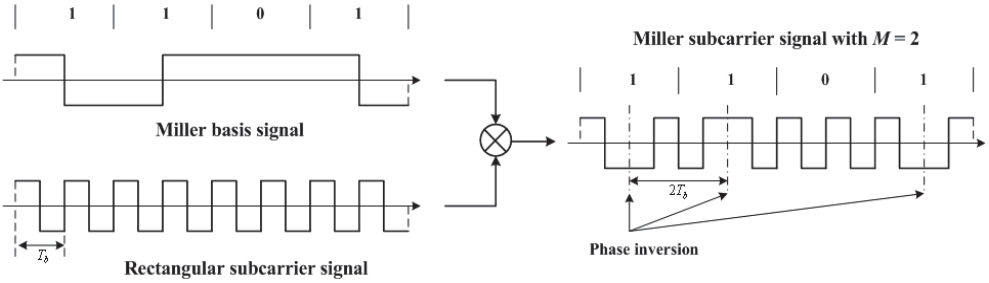

Fig. 2. Configuration of the Miller subcarrier signal with M = 2

In the second step, the created initial peak signal $r_{p1}(t)$ is reconstructed by removing the low level noise included in the specific level of the initial peak signal. This operation is implemented in the level decision block by using a reference level r_{ref} (Fig. 3). The reference level for the level decision is fixed at a value of 0. This is because the two orthogonal basis functions $s_{m0}(t)$ and $s_{m1}(t)$ participate in building the peak signal through Eq. (2), while only one basis function is used for the generation of the edge signal for the case of the FM0 signal [14]. Therefore, the demodulation method of the Miller subcarrier signal has the advantage that there is no need to find the optimal decision level, unlike the adaptive level decision method in the case of the FM0 signal. Then, the final peak signal can be obtained after the level decision by using the fixed reference level and the initial peak signal as follows:

$$r_{p2}(t) = \begin{cases} r_{p1}(t), & r_{p1} \geq r_{ref}(=0) \\ 0 \quad , & r_{p1} < r_{ref}(=0) \end{cases} \tag{5}$$

In the next step, from the final peak signal, $r_{p2}(t)$, the peak extractor (Fig. 3) finds the positions of the peaks using a peak detection algorithm which is identical to that of the edge extractor in Fig. 5 [14]. Finally, in the signal reconstruction block (Fig. 3), the basedband signal without DC-offset noise is regenerated by a state diagram which is also identical to that of the signal reconstruction block in Fig. 6 [14]. Therefore, the procedure for the proposed Miller subcarrier demodulation algorithm can be summarized as shown in Fig. 5

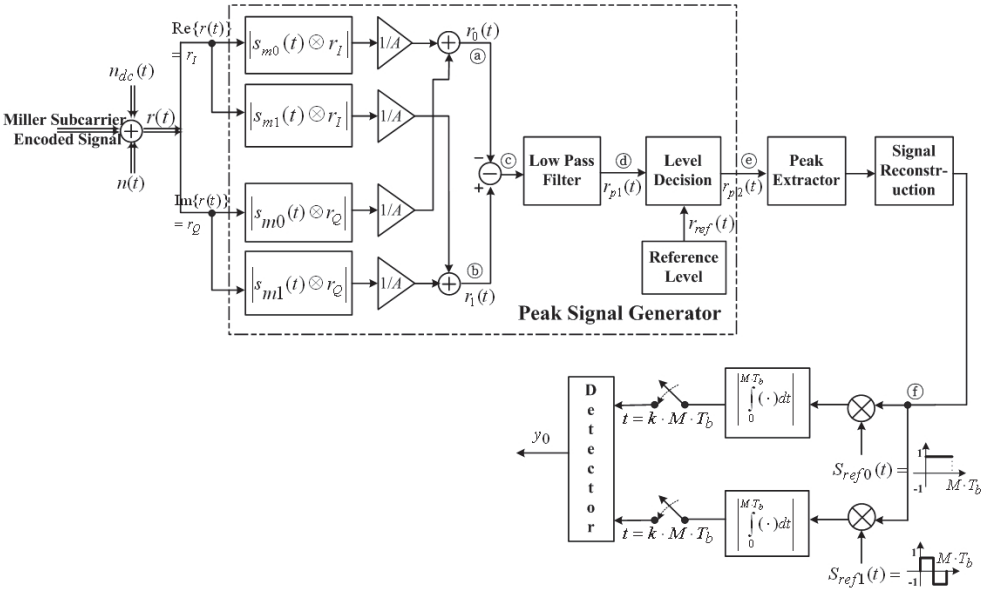

Fig. 3. Proposed demodulation structure for the purpose of reconstructing the Miller subcarrier signal distorted by DC-offset noise

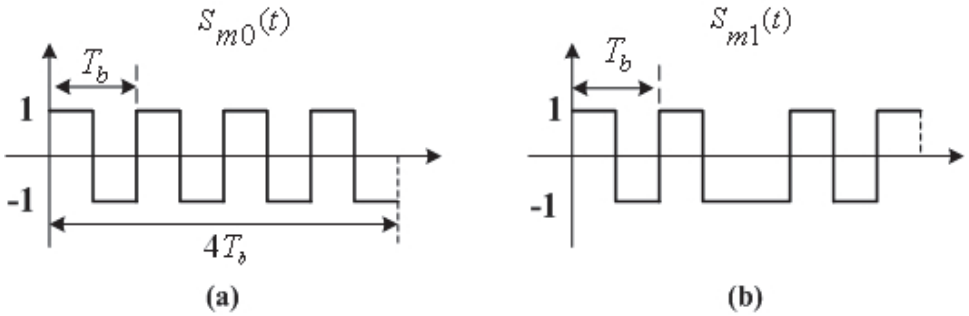

Fig. 4. Description of the two orthogonal basis functions, $s_{m0}(t)$ and $s_{m1}(t)$

2.2 Determination of the low pass filter specification

In our method for the demodulation of the Miller subcarrier signal, the difference signal between $r_1(t)$ and $r_0(t)$ must be reformed using a low pass filter (LPF), as mentioned in

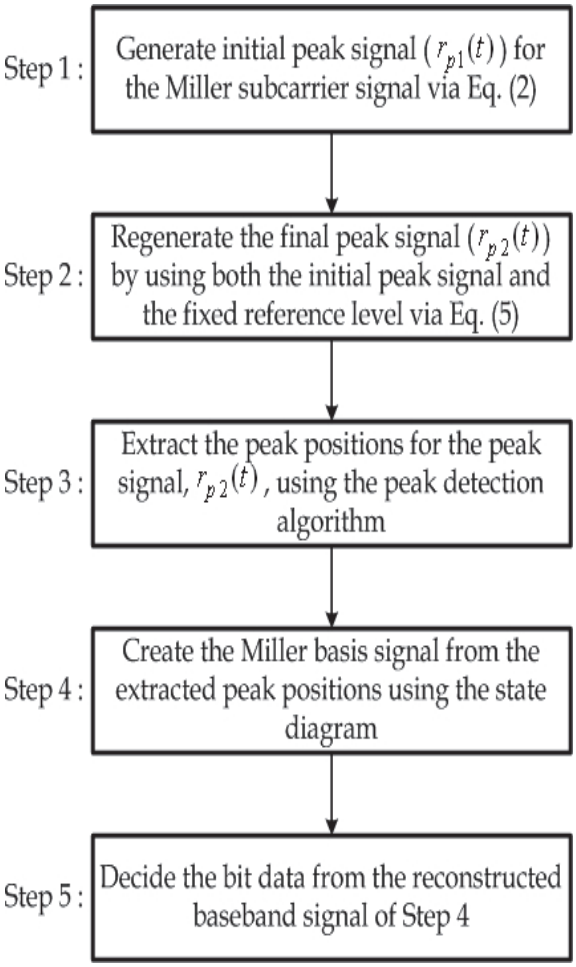

Fig. 5. Flowchart illustrating the Miller subcarrier demodulation method

Section 2.1. Fig. 6(a) shows the spectral response of the difference signal of the Miller subcarrier signal with M = 4 before the LPF, and Fig. 6(b) represents the spectral response of the initial peak signal $r_{p1}(t)$ after the LPF. To obtain the peak signal from the difference signal before the LPF, the second harmonic component of the difference signal (Fig. 6(a)) must be attenuated below a certain level, as shown in Fig. 6(b). We observe in Fig. 7 that, as the attenuation level Att_{dB} is increased, the error rate performance (p_e) for the Miller subcarrier signal is improved. However, the computational complexity for the design of the filter is also increased. This is because the order of the designed filter is increased to obtain the high level of the Att_{dB} . Meanwhile, when the Att_{dB} increase to a value larger than about 70dB, there is no noticeable improvement of the error rate performance. From the result shown in Fig. 7, we found that a level of attenuation Att_{dB} ranged from 70dB to 80dB can provide a suitable tradeoff between the computational complexity and the error rate

performance for the demodulation algorithm. The result in Fig. 6(b) was obtained using a 39th order LPF with an attenuation level of 70dB and the magnitude response of the designed LPF is shown in Fig. 8

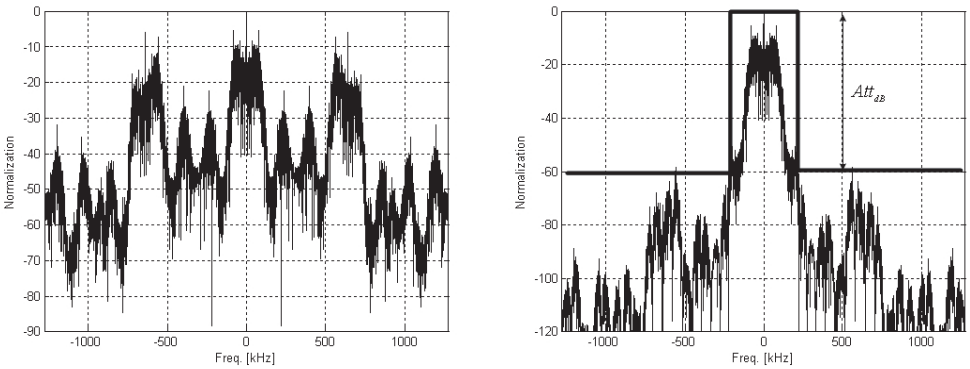

Fig. 6. Spectral responses of the difference signal before LPF (a) and the initial peak signal after LPF (b) (320kHz-Miller subcarrier signal with M = 4)

3. Simulation & experimental results

For the first example, we consider the operation of the proposed demodulation structure when the received baseband signal is the distorted Miller subcarrier-encoded signal with DC-offset noise (A_{dc} = 5, B = $T_s / T_b \cdot 100$, and w_d = $1/(T_b \cdot 100)$). Fig. 9 shows the demodulation result of the Miller subcarrier signal with M = 2. Case 1 of Fig. 9(a) and Case 2 of Fig. 9(b) represent the output signals $r_0(t)$ in Eq. (3) and $r_1(t)$ in Eq. (4), respectively. From the results, we observe that both output signals, $r_0(t)$ and $r_1(t)$, are robust to the variation of the amplitude, although the I- and Q-channel received baseband signals are severely distorted by DC-offset noise. Fig. 9(c) represents the difference signal between $r_1(t)$ and $r_0(t)$ and the corresponding initial peak signal after the LPF. A 54th order LPF is designed for the generation of the initial peak signal $r_{p1}(t)$, in order to attenuate the amplitude response of the filter to about 80dB. The spectral responses of the difference signal before the LPF and the initial peak signal after the LPF, and the magnitude response of the designed 54th order LPF are shown in Fig. 10. Fig. 9(d) represents the final peak signal $r_{p2}(t)$ using the fixed reference level of 0 and the initial peak signal $r_{p1}(t)$. Note that the generated peaks of $r_{p2}(t)$ are placed at every position at which a phase inversion occurs within the Miller subcarrier signal sequence. Finally, as shown in Fig. 9(e), the reconstructed baseband signal without the DC-offset noise is obtained using the peak extraction algorithm of the peak extractor and the state diagram of the signal reconstruction block. The resulting signal in Fig. 9(e) has the same form as the Miller basis signal, which is obtained by removing the rectangular subcarrier signal from the Miller subcarrier signal, as shown in Fig. 2. This is because the peak signal $r_{p2}(t)$, which appears at a position having phase inversion, is used to reconstruct the Miller baseband signal.

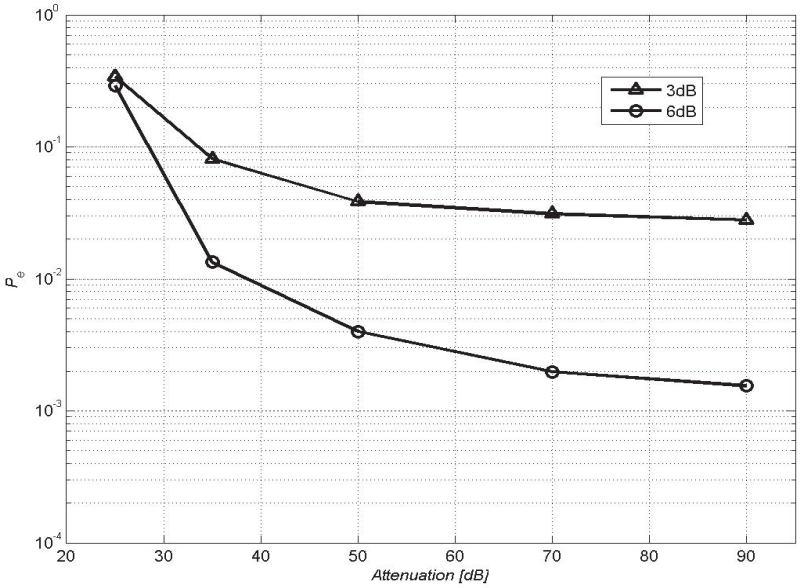

Fig. 7. The error rate performances for several values of Att_{dB}

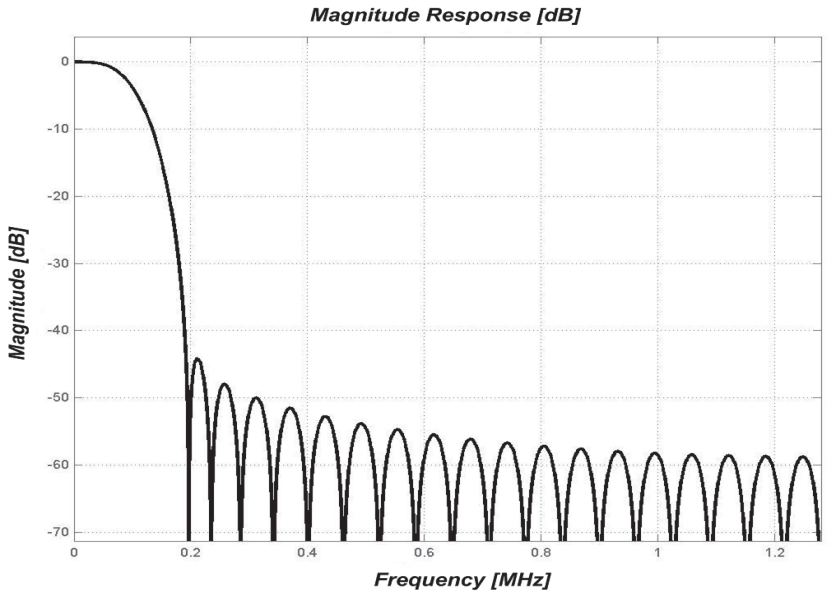

Fig. 8. The magnitude response of the designed 39th order low-pass filter for the generation of the initial peak signal

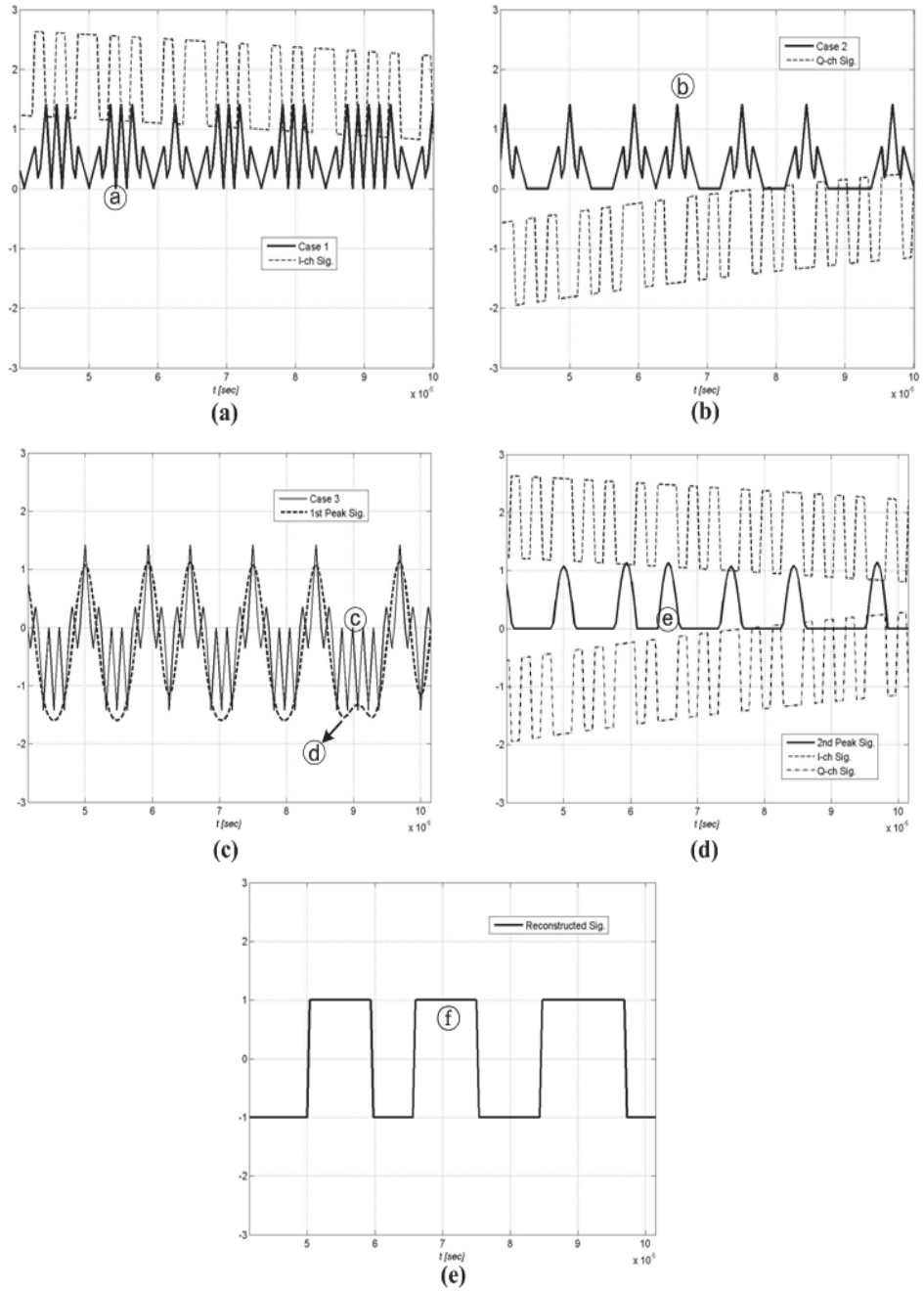

Fig. 9. Operation results of the proposed demodulation structure shown in Figure 3 (320kHz-Miller subcarrier signal with M = 2)

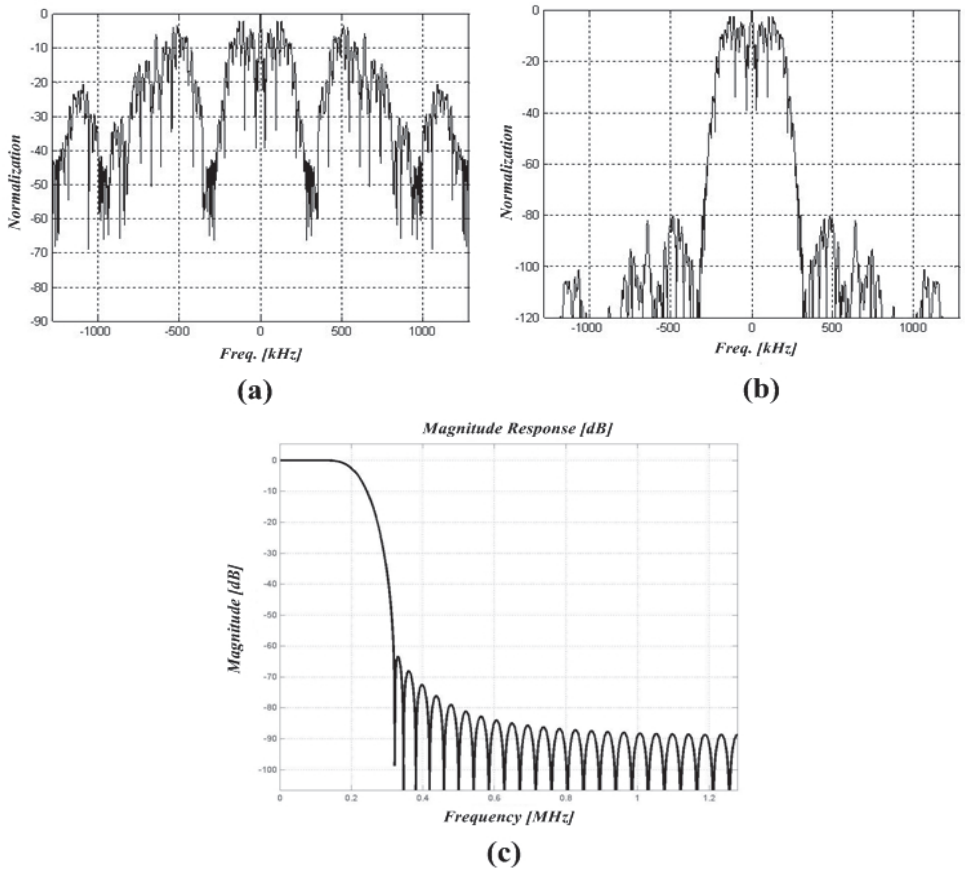

Fig. 10. Spectral responses of the difference signal before LPF (a) and the initial peak signal after LPF (b), and the magnitude response of the designed 54th order LPF (c) (320kHz-Miller subcarrier signal with M = 2)

For the second example, the Miller subcarrier signal with M = 4 is considered for the signal reconstruction, as shown in Fig. 11. The descriptions of Fig. 11 are explained as follows:
Case 1: the output signal $r_0(t)$ in Eq. (3) using $s_{m0}(t)$
Case 2: the output signal $x_1(t)$ in Eq. (4) using $s_{m1}(t)$
Case 3: the difference signal between $r_1(t)$ and $r_0(t)$ before the 39th order LPF having an attenuation level of 70dB
Case 4: initial peak signal $r_{p1}(t)$ after the 39th order LPF
Case 5: final peak signal $r_{p2}(t)$ using the fixed reference level and the initial peak signal $r_{p1}(t)$
Case 6: Reconstructed Miller baseband signal without DC-offset noise

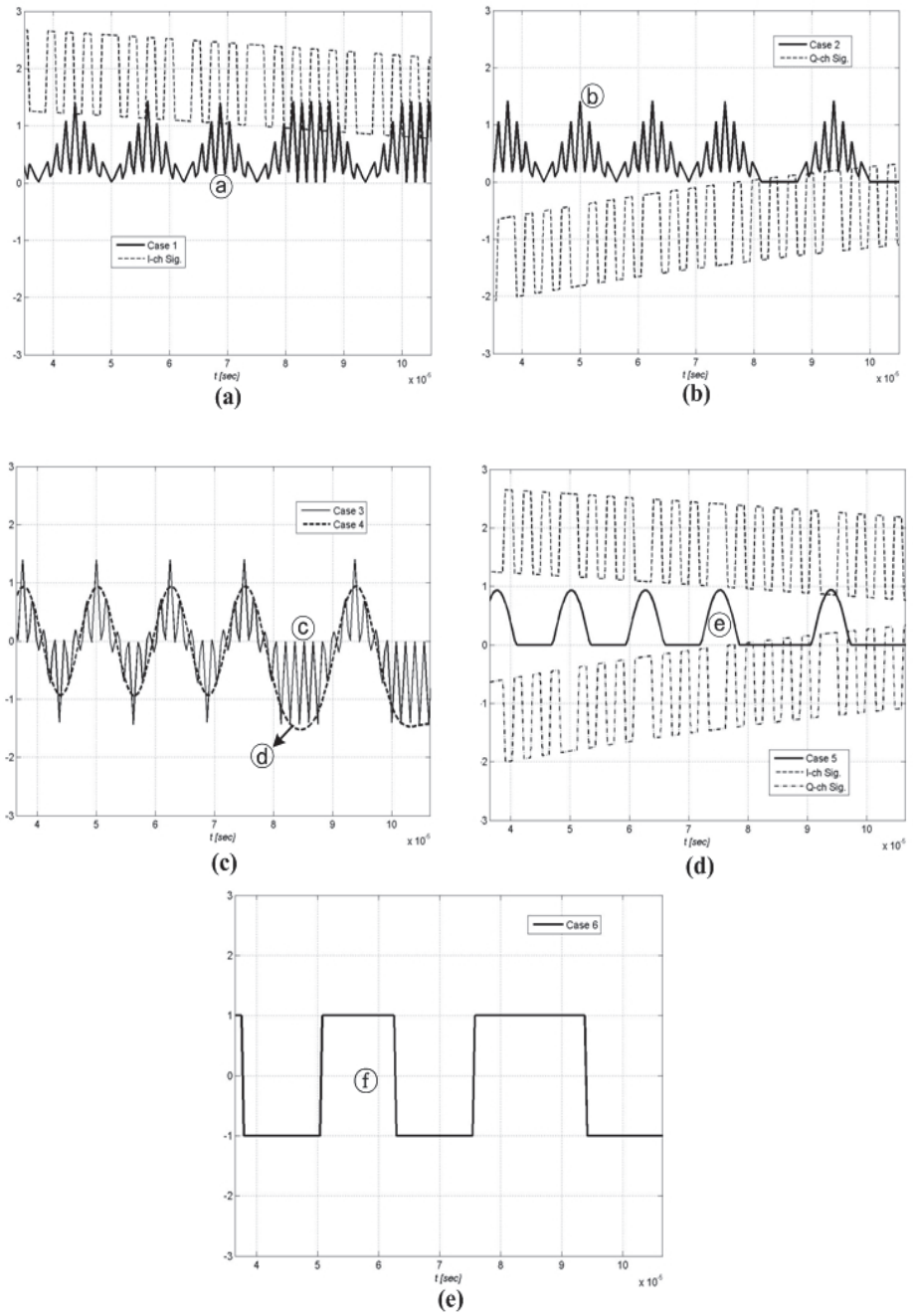

Fig. 11. Operation results of the proposed demodulation structure shown in Figure 3 (320kHz-Miller subcarrier signal with M = 4)

In the next example, we implemented the proposed demodulation structure as a hardware device FPGA (Field Programmable Gate Array) and then the operation of the demodulation structure is observed using the commercial DSP design tool, Xilinx System Generator which provides hardware co-simulation, making it possible to incorporate the demodulation design running in an FPGA directly into a MATLAB Simulink simulation [15]. Fig. 12 shows the designed hardware co-simulation model of the proposed demodulation structure using a Black Box and JTAG Co-Sim library block provided by the System Generator. The Black Box library block allows a designed HDL (hardware description language), such as VHDL and Verilog, to be brought into the Simulink design model and enables us to easily observe the corresponding simulation behaviour in MATLAB Simulink.
In order to execute the designed Simulink model of the demodulation structure in Fig. 12, the following hardware co-simulation environment should be considered as shown in Table 1.

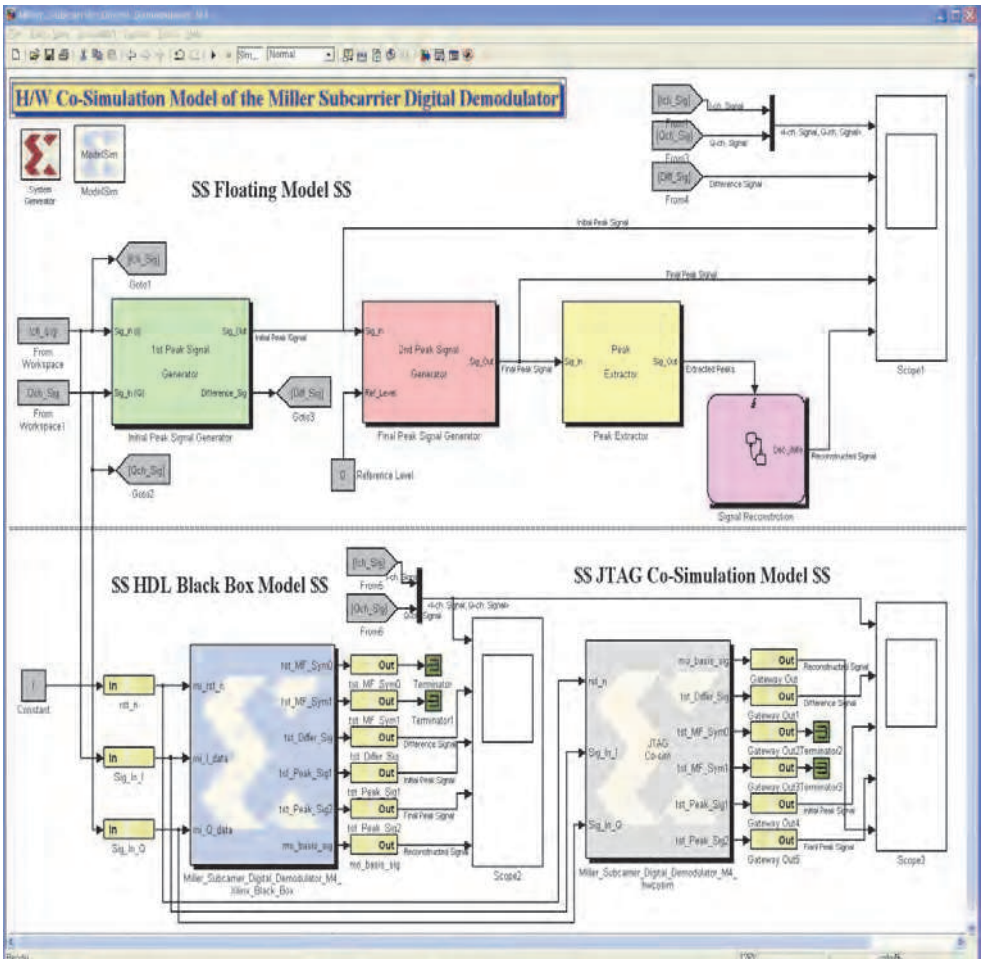

Fig. 12. Hardware co-simulation model with Black Box and JTAG Co-Sim library block

Items	Descriptions
MATLAB	MATALB 2008a
System Generator	Xilinx System Generator 10.1
HDL design tool	Xilinx ISE 10.1
HDL simulation tool	ModelSim SE 6.2b
FPGA (Digital hardware board)	Xilinx SPARTAN-3 XC3S4000FGG676-5G
JTAG Cable	Xilinx USB cable
Simulink system period [sec]	3.90625e-7 (1/2.56MHz)

Table 1. Hardware co-simulation configuration for the verification of the demodulation structure

Meanwhile, the Black Box HDL can be co-simulated with MATLAB Simulink using the System Generator interface to either ISE simulator or the ModelSim simulation software from Model Technology, Inc. Fig. 13 shows the operation result of the demodulation structure using the latter method through ModelSim when the measured Miller subcarrier signal (Fig. 2(b)) is considered. The operation result (Scope 2) using the former method through ISE simulator is also shown in Fig. 14

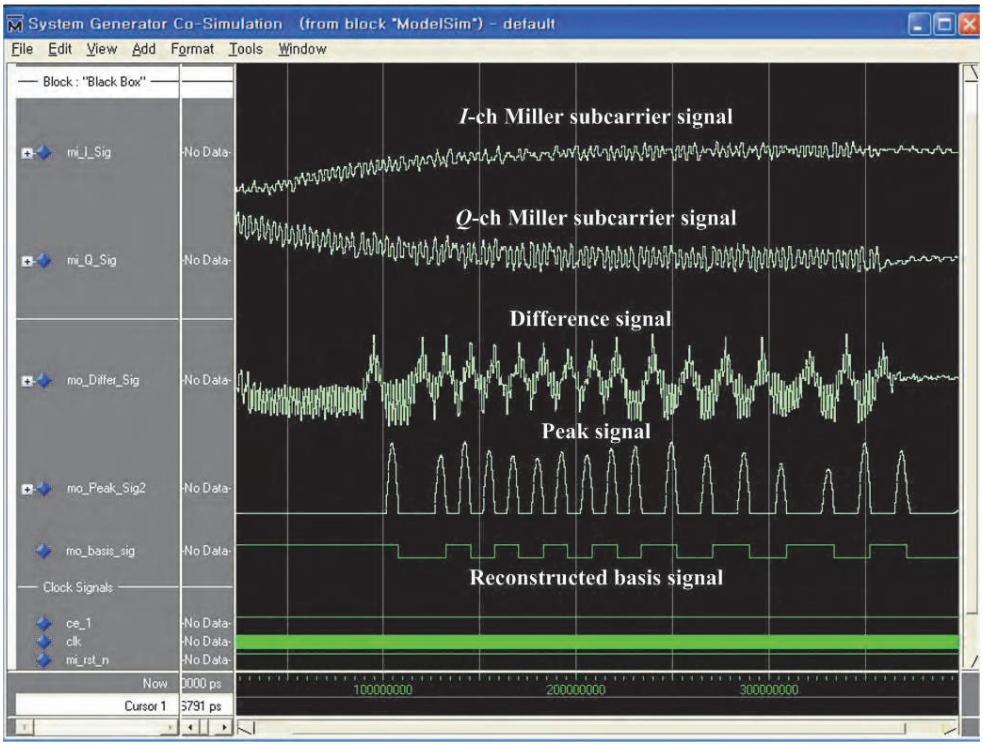

Fig. 13. Simulation result showing Black Box output through ModelSim for the proposed demodulation structure

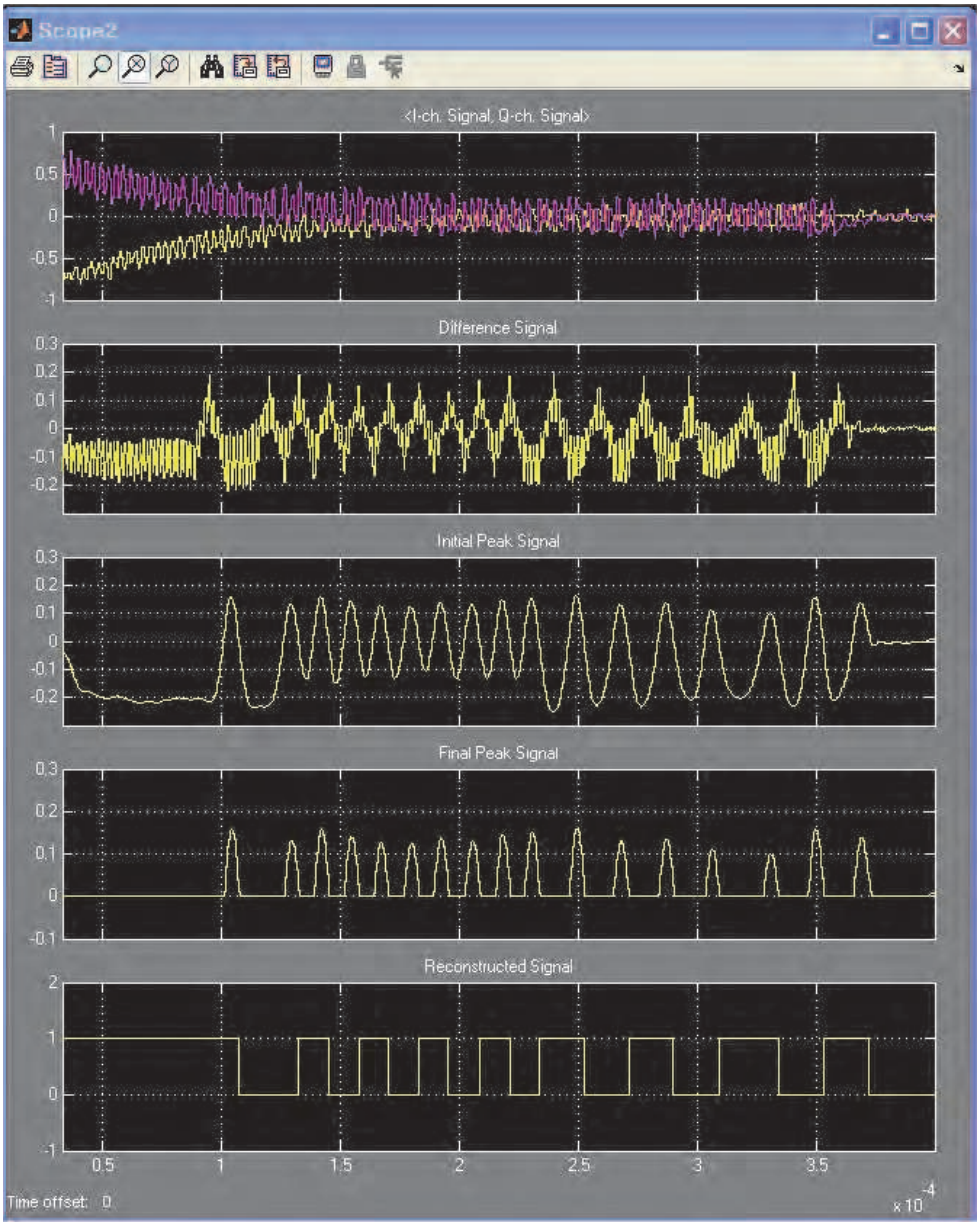

Fig. 14. Simulation result showing Black Box output through ISE simulator for the proposed demodulation structure

Next, Fig. 15 shows the hardware co-simulation result in Scope 3 when the same measured Miller subcarrier signal (Fig. 2(b)) is considered.

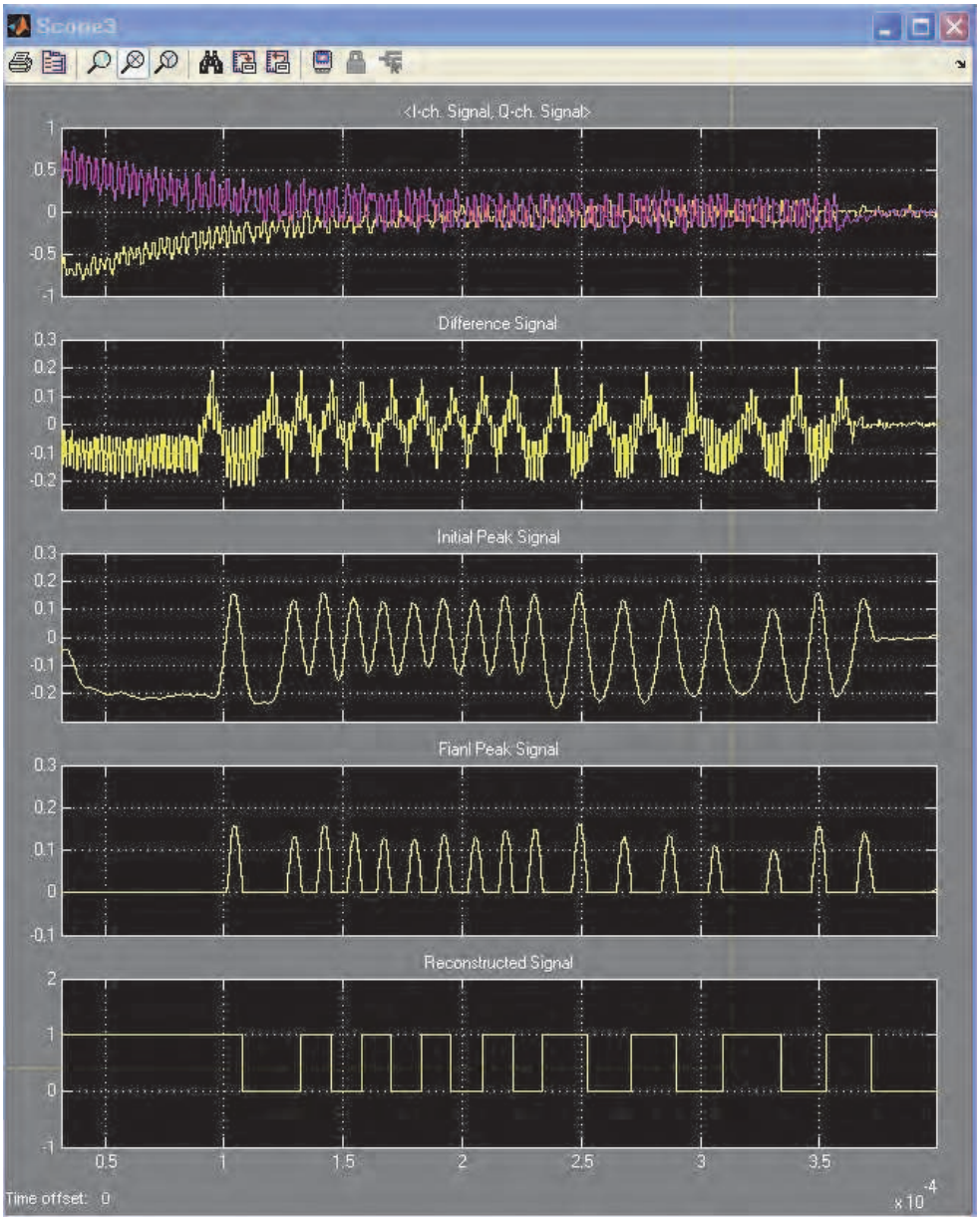

Fig. 15. Simulation result showing JTAG Co-Sim block output for the proposed demodulation structure

To obtain the JTAG Co-Sim library block (Fig. 12) for the demodulation structure, the hardware and software required to run the hardware co-simulation on the FPGA board (Table 1) should be installed and set up in advance [15]. Therefore, once the System

Generator has successfully finished compiling the HDL design into the FPGA bitstream, it automatically creates the JTAG Co-Sim library block as shown in Fig. 12. As a result, in comparison with Fig. 14, we observe that the timing simulation result of Fig. 15 is nearly identical to the functional HDL simulation result of Fig. 14.
Finally, the measured operation results obtained using Agilent Logics Analyzer equipment are described in Fig. 16. From the results of Figs. 13, 14, 15, and 16, we observe that the proposed method can successfully reconstruct the Miller baseband signal, even though the received Miller subcarrier signal is distorted by the DC-offset phenomenon. Although we do not show the corresponding demodulation results, the demodulation structure and algorithm described in Section 2 can be directly used to reconstruct a distorted Miller subcarrier signal with $M = 8$.

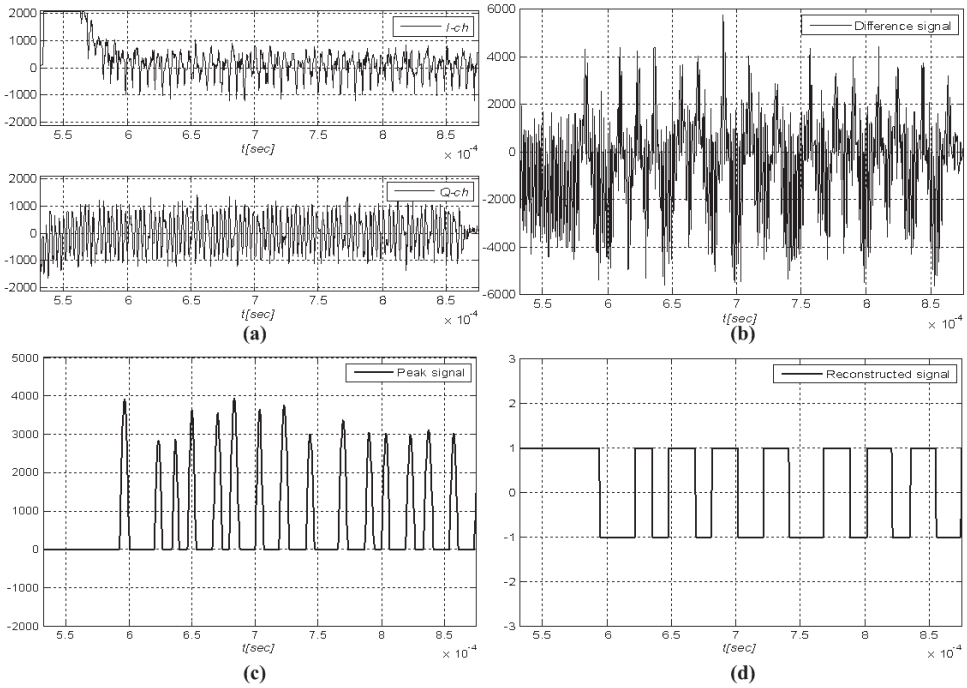

Fig. 16. Experimental results of the proposed Miller subcarrier demodulation structure (320kHz-Miller subcarrier signal with $M = 4$)

3. Conclusion

In this study, we propose a reader baseband receiver structure for the demodulation of the Miller subcarrier signal described in the international UHF RFID standard, 18000-6 Type C, under the DC-offset phenomenon. In order to perfectly remove the DC-offset noise caused by the leakage components in a passive RFID environment, the proposed structure for the passive RFID reader baseband receiver primarily includes the peak signal generator, the peak extractor, and the signal reconstruction block for demodulating Miller subcarrier

signals. The phase inversion information is used to generate the peak signal and the resulting reconstructed signal is the Miller baseband signal removed both the DC-offset noise and the rectangular subcarrier signal simultaneously. To verify the operation and functionality of the proposed demodulation structure, we implemented both the HDL co-simulation using the Black Box library block and the hardware co-simulation using the JTAG Co-Sim one simultaneously. The results show that the proposed demodulation method can successfully extracts the valid information from the signal corrupted by the DC-offset noise which can occur in a passive RFID configuration.

4. Acknowledgment

This work was supported by the IT R&D program of MKE/IITA [Development of Next Generation RFID Technology for Item Level Applications], Rep. of Korea.

5. References

[1] Finkenzeller, K., "RFID Handbook – Fundamentals and Applications in Contactless Smart Cards and Identification", John Wiley & Sons Ltd, 2003.

[2] Daniel M. Dobkin, "The RF in RFID", Elsevier Inc., 2008.

[3] "Radio-Frequency Identification for Item Management – Part 6: Parameters for Air Interface Communications at 860MHz to 960MHz", ISO/IEC 18000-6 Type C, 2009.

[4] H.-W. Son, J.-N. Lee, and G.-Y. Choi, "Design of Compact RFID Reader Antenna with High Transmit/Receive Isolation", Microwave and Optical Technology Letters, Vol. 48, No. 12, Dec., 2006.

[5] Scott Chiu, et al.,"A 900MHz UHF RFID Reader Transceiver IC", IEEE Journal of Solid-State Circuits, Vol.42, No.12, December, 2007.

[6] Jeiyoung Lee, et al., "A UHF Mobile RFID Reader IC with Self-Leakage Canceller", IEEE Radio Frequency Integrated Circuits Symposium, pp.273~pp.276, 2007.

[7] Fan Z. G., S. Qiao, J.T. Huangfu, and L.X.Ran, "Signal descriptions and formulations for long range UHF RFID readers", Progress In Electromagnetics Research, Vol. 71, pp.109-127, 2007.

[8] Harrison B. Chung, et al.,"An advanced RFID system to avoid collision of RFID reader, using channel holder and dual sensitivities", Microwave and Optical Technology Letters, Vol. 49, No. 11, Aug., 2007.

[9] WonKyu Choi, et al., "RFID Tag Antenna Coupled by Shorted Microstrip Line for Metallic Surfaces", ETRI Journal, Vol. 30, No. 4, August 2008.

[10] Ickjin Kwon, "A Single-Chip CMOS Transceiver for UHF Mobile RFID Reader", IEEE Journal of Sold-State Circuits, Vol. 43, No. 3, March 2008.

[11] Ki Yong Jeon, and Sung Ho Cho, "A RFID EPC C1 Gen2 System with Channel Coding Capability in AWGN Noise Environments", IEICE Trasn. Commun., Vol. E92-B, No.2, Feb. 2009.

[12] Ah. Wasif Reza, and T. K. Geok, "Objects tracking in a dense reader environment utilizing grids of RFID antenna positioning", International Journal of Electronics, vol.96, no. 12, pp.1281~pp.1307, 2009.

[13] Iker Mayordomo, et al.,"Design and Implementation of a Long-Range RFID Reader for Passive transponders", IEEE Trans. On Microwave theory and tech. Vol. 57, No. 5, May, 2009.

[14] J.-H. Bae, et al.,"Study on the demodulation structure of a reader receiver in a passive RFID environment", Progress In Electromagnetics Research, Vol. 91, pp.243-258, 2009.

[15] "System Generator for DSP, User Guide", Xilinx Inc., Sept., 2008.

Current Trends and Challenges in RFID

Edited by Prof. Cornel Turcu

ISBN 978-953-307-356-9
Hard cover, 502 pages
Publisher InTech
Published online 20, July, 2011
Published in print edition July, 2011

With the increased adoption of RFID (Radio Frequency Identification) across multiple industries, new research opportunities have arisen among many academic and engineering communities who are currently interested in maximizing the practice potential of this technology and in minimizing all its potential risks. Aiming at providing an outstanding survey of recent advances in RFID technology, this book brings together interesting research results and innovative ideas from scholars and researchers worldwide. Current Trends and Challenges in RFID offers important insights into: RF/RFID Background, RFID Tag/Antennas, RFID Readers, RFID Protocols and Algorithms, RFID Applications and Solutions. Comprehensive enough, the present book is invaluable to engineers, scholars, graduate students, industrial and technology insiders, as well as engineering and technology aficionados.

How to reference

In order to correctly reference this scholarly work, feel free to copy and paste the following:

Ji-Hoon Bae, Kyung-Tae Kim, WonKyu Choi and Chan-Won Park (2011). Design and Implementation of Reader Baseband Receiver Structure in a Passive RFID Environment, Current Trends and Challenges in RFID, Prof. Cornel Turcu (Ed.), ISBN: 978-953-307-356-9, InTech, Available from: http://www.intechopen.com/books/current-trends-and-challenges-in-rfid/design-and-implementation-of-reader-baseband-receiver-structure-in-a-passive-rfid-environment

INTECH
open science | open minds

InTech Europe
University Campus STeP Ri
Slavka Krautzeka 83/A
51000 Rijeka, Croatia
Phone: +385 (51) 770 447
Fax: +385 (51) 686 166
www.intechopen.com

InTech China
Unit 405, Office Block, Hotel Equatorial Shanghai
No.65, Yan An Road (West), Shanghai, 200040, China
中国上海市延安西路65号上海国际贵都大饭店办公楼405单元
Phone: +86-21-62489820
Fax: +86-21-62489821